Received: 12 April 2024 | Revised: 16 May 2024 | Accepted: 5 August 2024

DOI: 10.1111/vru.13425

ORIGINAL RESEARCH

WILEY

Ex vivo MRI and histological comparison of the canine adrenal glands

Olga Amorós Carafí[1] | Michelle Imlau[2,3] | Giulia Dalla Serra[1] | Antonella Puggioni[1] | Eimear Shorten[1] | Brain Cloack[4] | Seamus Hoey[1]

[1]Department of Diagnostic Imaging, University College Dublin Veterinary Hospital, Belfield, Ireland

[2]Pathobiology Section, University College Dublin Veterinary Hospital, Belfield, Ireland

[3]Department of Infectious Diseases and Pathobiology, University of Bern Institute for Fish and Wildlife Health, Bern, Switzerland

[4]Department of Pathology, University College Dublin Veterinary Hospital, Belfield, Ireland

Correspondence
Olga Amorós Carafí, Department of Diagnostic Imaging, University College Dublin Veterinary Hospital, Belfield D04 W6F6, Dublin, Ireland.
Email: olga.amoroscarafi@ucdconnect.ie

Abstract

Cross-sectional imaging is widely used to characterize adrenal gland tumors in humans. In small animal veterinary medicine, while some studies have attempted to distinguish between types of adrenal gland neoplasia using CT, peer-reviewed studies investigating canine adrenal glands on MRI are scant. This prospective, pilot, single-center, method comparison, cadaveric study aimed to assess the agreement between ex vivo MRI findings and analogous histopathological findings of the adrenal glands in dogs. The adrenal glands of randomly selected dogs presented for necropsy were examined by MRI (n = 31). Additionally, five adrenal masses in dogs who underwent invasive adrenalectomy (including three adrenocortical carcinomas, one pheochromocytoma, and one adenoma) were imaged. Subsequently, gross pathology and histopathology of all the specimens were performed and correlated with the imaging findings. Adrenal gland lesions were identified on MRI with a sensitivity of 24%, a specificity of 100%, a positive predictive value of 100%, a negative predictive value of 31%, and an accuracy of 45%. The present study provides MRI features of multiple adrenal gland lesions that had never been described in dogs, including cortical hyperplasia, nodular fibrosis, hemorrhage, or multiple tumors, such as adenoma, carcinoma, and hemangiosarcoma. While MRI identified numerous adrenal gland lesions, a significant portion of those went undetected. Therefore, the absence of adrenal gland lesions on MRI does not exclude the possibility of histological lesions being present.

KEYWORDS
diagnosis, dog, endocrine, histology, pheochromocytoma

1 | INTRODUCTION

Primary adrenal gland neoplasia accounts for 0.17–0.76% of all tumors in dogs.[1] Cortical adenoma and adenocarcinoma are the most common adrenal tumors identified, followed by medullary pheochromocytoma. The treatment of choice for adrenal tumors is often surgical adrenalectomy; however, perioperative complications and mortality rates vary greatly depending on the type of neoplasm.[1]

Adrenal masses are often found incidentally in human cross-sectional abdominal studies, with an estimated prevalence of 0.35–5%.[2,3] The distinction between benign and malignant human adrenal lesions is of fundamental importance for prognostic assessment and for determining the appropriate therapeutic approach.[3]

Advanced imaging modalities play an important role in characterizing adrenal tumors. The majority of detected adrenal masses are adenomas.[2] There are two types of adrenal adenomas based on the amount of lipids that they contain. Lipid-rich adenomas contain a large amount of intracellular lipids and are the most common type, accounting for 70% of all of them. Due to their high lipid content, they show low attenuation values on non-contrast CT (<10 Hounsfield Units (HU)), which makes their diagnosis uncomplicated. Lipid-poor adenomas are less common and typically display attenuation values over 10 HU, similar to other types of malignant neoplasia. Both types of adenomas tend to have a rapid wash-out when intravenous contrast is administered. This additional imaging feature differs from other malignant neoplasia, which displays a more delayed wash-out of contrast.[2] In one study, the rapid wash-out of contrast allowed the differentiation of adenomas from other neoplasia with a sensitivity and specificity as high as 100% and 98%, respectively.[4] When the diagnosis remains inconclusive or CT is not indicated (for example, in pregnant or breastfeeding women), MRI is the modality of choice. The use of MRI has increased in recent years due to the advantages of avoiding radiation exposure, as well as the superior signal-to-noise ratio (SNR) and contrast-to-noise ratio (CNR) compared with CT. Similar to CT, specific MRI protocols facilitate differentiating adenomas from malignant adrenal tumors, with a reported sensitivity of 87% and a specificity of 95%.[5] A specific sequence commonly used in humans for this purpose is chemical shift imaging (CSI), which is capable of depicting microscopic fat typical of adenomas.[5,6]

In veterinary medicine, while some studies have attempted to distinguish between types of adrenal neoplasia using CT,[1,7] peer-reviewed studies investigating canine adrenal glands on MRI are scant. The imaging features of presumed normal canine adrenal glands on high-field MRI were described in 2003.[8] More recently, one study described the MRI appearance of the adrenal glands in 6 research beagle dogs using different pulse sequences using a 3 Tesla (T) unit.[9] However, there is a paucity of information available on the MRI appearance of the abnormal adrenal glands. A single case report in a dog with an adrenal pheochromocytoma has been reported on MRI,[10] but other types of adrenal tumors have not been described. Moreover, studies describing a comparison between MRI and histologic characteristics of canine adrenal glands are lacking. Consequently, the present study aimed to assess the agreement between ex vivo MRI findings and analogous histopathological findings of the adrenal glands in dogs. The hypothesis was that a 1.5 T MRI of ex vivo adrenal glands would show a strong correlation with histopathologic findings.

2 | MATERIALS AND METHODS

2.1 | Case selection

This prospective, comparative, pilot study was approved by the Animal Research Ethics Committee of University College Dublin (AREC-E-20-38-Hoey). Canine cadavers presented for necropsy to the anatomic pathology section of the UCD Veterinary Hospital between September 2021 and July 2022 were included regardless of signalment. Dogs were excluded if the adrenal glands were injured during the necropsy examination.

During the same time-period, adrenal glands from patients undergoing elective surgical adrenalectomy for adrenal masses were imaged and examined histologically.

Demographic data, including breed, sex, weight, and cause of death, were recorded.

2.2 | Anatomic study

Each canine cadaver underwent a routine necropsy examination supervised by a European College of Veterinary Pathology (ECVP) Resident or Diplomate. All adrenal glands were resected and placed in 10% neutral buffered formalin for at least 24 hours prior to MRI examination.

Following imaging, each adrenal specimen was sectioned in a sagittal plane, halving the adrenal glands. For histological examination, the adrenal gland specimens were embedded in paraffin, sectioned at 4 μm, and stained with hematoxylin and eosin using a standard histologic technique. All samples were examined under light microscopy by an ECVP diplomate (M.I.). When pathological findings were encountered, those were described, and a final histological diagnosis was established.

The adrenal glands from dogs that underwent surgical adrenalectomy were also imaged and processed for histology. However, those adrenal glands were not included in the statistical analysis.

2.3 | Data imaging recording

In order to establish a preliminary imaging protocol, several human and veterinary publications were consulted (Table 1).[5,6,8,11] Magnetic resonance imaging studies were performed by a board-certified veterinary radiologist (O.A.) using a 1.5 Tesla MRI unit (General Electric HealthCare Signa Artist) and a small flex coil. Each adrenal specimen was imaged individually. All adrenal gland specimens were positioned with the cranial pole toward the magnet and placed on a sheet of saline-moistened tissue paper to safeguard the coils. A pilot protocol was developed on examination of the first three adrenal specimens, which was ultimately used to establish a definitive MRI protocol (Table 1). These three specimens were not included in statistical analysis. Specific technical factors for the different planes and sequences used on MRI are detailed in Table 2.

2.4 | MRI description of the findings and correlation with histopathology

All MRI studies were reviewed by a board-certified veterinary radiologist (O.A.) who was aware of the signalment and the final diagnosis at the time of MRI analysis. The imaging findings were then compared with the histological findings together with a board-certified

TABLE 1 MRI protocols used to scan the abdomen in humans and dogs, proposed by different authors.

	Llabrés-Diaz et al.[8]	Manley et al.[11]*	Adam et al.[5]	d'Amuri et al.[6]	Proposed, 2024
T2W	T, D, S		T, D	T, D	T, D, S
T1W pre- and postcontrast	T, D, S				T, D (precontrast)
DWI			T	T	
T1W GE	T, S	T			
T1W FSPGE (3D LAVA) pre- and postcontrast			T	T	T (precontrast)
T2W FS		D		T	T, D
T1W IDEAL (Dixon)					T, D
Dual Echo			T, D	T	T
T2*					T

Note: In some of the protocols (*) the sequences reported to be of limited image quality on the respective studies are not indicated.Abbreviations: 3D LAVA, three-dimensional liver acceleration volume acquisition; D, dorsal; DWI, diffusion-weighted image; FS, fat saturation; FSPGE, fast spin gradient echo; GE, gradient echo; IDEAL, iterative decomposition of water and fat with echo asymmetry and least-square estimation; S, sagittal; T, transverse; T2*, T2 star (this sequence was only used in the 5 dogs that underwent surgical adrenalectomy).

TABLE 2 Sequences and parameters used for the evaluation of the adrenal gland specimens with a 1.5-Tesla MRI unit.

Pulse sequence	Plane	TE (ms)	TR (ms)	Slice thick (mm)	Interslice gap (mm)	N° slices	FOV	Time (min)	SNR	NEX	Flip angle
T2W FSE	Sagittal	82	2546	1.5	0.3	9	13	2:26	83	4	
	Dorsal	84	2513	1.5	0.3	9	13	2:07	84	4	
	Transverse	87	3978	1.5	0.3	18	12	3:40	83	4	
T1W IDEAL	Dorsal	14	467	1.5	0.3	9	13	4:39	83	1.2	
	Transverse	13	541	1.5	0.2	20	16	5:02	87	1.2	
T2W FSE FS	Dorsal	84	2526	1.5	0.3	9	13	2:12	93	3.7	
	Transverse	82	4205	1.5	0.3	19	13	3:24	80	3.4	
T1W SE	Dorsal	10	400	1.5	0.3	9	13	4:11	99	3	
	Transverse	15	499	1.5	0.3	19	13	3:40	87	3	
3D Lava	Transverse	4	11	2	0.3	–	13	4:06	99	1	12
Dual-echo	Transverse	4/8	180	1.9	0.3	12	11	0:51	95	1	70

Note: The values indicated here are the means of values used for each specimen.
Abbreviations: FOV, field of view; NEX, number of excitations; SNR, signal-to-noise ratio; TE, time to echo; TR, time to repetition.

veterinary pathologist (M.I.). The description of a normal adrenal gland on MRI was defined in agreement between the two authors (O.A. and M.I.). Adrenals were considered normal if tubular in shape, but with a variable appearance of their poles. Adrenals were normal in the absence of nodules or masses. As described in a relevant pathology textbook,[12] and anecdotally, smoothly marginated projections or invaginations from the cortex into the medulla were considered a normal anatomical variant. The cortex and medullary thickness were evaluated subjectively, and a ratio of approximately 2–4:1 was considered normal.[13] The signal intensity of the cortex and the medulla was evaluated in the different sequences. When adrenal nodules or masses were identified, the size, shape, and signal intensity were assessed. Moreover, the adrenal signal intensity index on the dual-echo sequence was calculated as previously described in human literature using the following formula: [(signal intensity on in-phase imaging)−(signal intensity on opposed-phase imaging)/(signal intensity on in-phase imaging)] × 100%.[5] The signal intensities of the adrenal lesions were measured with an electronic cursor using circular regions of interest (ROI). The ROIs were chosen to cover the majority of the adrenal at the widest dimension. Necrotic, hemorrhagic, or calcified components of the mass were excluded from the region of interest whenever possible.[5,14] Adrenal gland measurements were performed by the first author (O.A.). Based on previous ultrasonographic and computed tomographic literature,[15–17] the caudal pole height was chosen as the site to measure the adrenal glands. The height of the caudal pole of all adrenal glands was measured at the greatest dimension perpendicular to the

longitudinal axis of the gland. The measurements were performed on a sagittal plane T2W sequence using freely available DICOM image viewing software (Horos Project), and each measurement was performed only once. The correlation between the height of the caudal pole and the patient's body weight was evaluated.

2.5 | MRI sequences quality assessment

For each adrenal gland, the MRI sequences were anonymized. Two observers, including one board-certified veterinary radiologist (A.P.) and a second-year radiology resident (G.D.S.) independently reviewed and scored the image quality of each of the MRI sequences. The observers were not aware of the signalment and the final diagnosis at the time of MRI analysis. Image analysis was performed using the same medical imaging software (Horos Project).

A novel 4-point scale scoring system was designed based on the ability to distinguish between the adrenal cortex and medulla on the different sequences (Supporting Information Materials). Grade 1 defined the adrenal cortex and medulla as being indistinguishable. Grade 2 defined the cortex and medulla as being minimally discernible and the cortex as not being reliably measurable or only measurable in a small region accounting for approximately ≤25% of the adrenal surface. Grade 3 defined good corticomedullary differentiation and cortical thickness measurement as possible in approximately 50% of the adrenal surface. Grade 4 defined a clear corticomedullary distinction, with the cortex being easy to measure in more than 75% of the adrenal surface. On rare occasions where the observers disagreed by more than two grades, the observers were asked if they wanted to maintain or change the elected category without revealing the choice of the other observer. This was performed to ensure that those discrepancies between scores were not due to an oversight error of one of the observers. The scores of the same sequence from each specimen were added together, and the sequence that obtained the highest outcome was considered best for corticomedullary differentiation. The scores of all sequences of the same adrenal gland were also added together to obtain an individual score. The effect of dogs' body weight and age on the ability to differentiate the cortex and the medulla was evaluated.

2.6 | Statistical analyses

Statistical analyses were carried out by the first author (O.A.) under the guidance of an external statistician with advanced training in research methods and statistics. All analyses were performed using statistical analysis software (IBM Corp. Released 2020. IBM SPSS, version 27.0). The means, ranges, ratios, percentages, and standard deviation were calculated using descriptive statistics. The correlation between body weight and adrenal gland height was estimated using Pearson's correlation analysis. The effect of body weight and age on the total score of each specimen was evaluated by nonparametric Spearman's rho. The level of significance was established as a *P*-value less than .05, and the confidence interval (CI) used was 0.95%.

3 | RESULTS

Initially, 33 dogs were included in the study. Two dogs were excluded due to accidental damage to the adrenal glands during the necropsy examination. Ultimately, 31 dogs were included, with a total of 62 adrenal glands. The mean age of the dogs was 5 years old (5 months–12 years old), and the mean body weight was 21 kg (1.25–38.5 kg). Twenty-one different breeds were included, and none of the breeds were overrepresented.

The sequence that was best graded for corticomedullary differentiation was the T2W-FATSAT sequence in the transverse plane, followed closely by T2W also in the transverse plane. The cortex and medulla could be differentiated on MRI in all adrenal glands and in the majority of sequences. On T2W sequences, the medulla was always hyperintense to the cortex, and corticomedullary differentiation was always possible. On T1W sequences, the medulla was hyperintense (58/62) or isointense (4/62) to the cortex, and corticomedullary differentiation was possible in all but four adrenal glands. The sequence that was graded poorest for corticomedullary differentiation was the dual-echo sequence, followed by the 3D LAVA sequence.

The mean height of the caudal pole of the right adrenal gland was 0.68 ± 0.17 cm. The mean height of the caudal pole of the left adrenal gland was 0.77 ± 0.19 cm. A moderate to strong positive correlation was found between adrenal gland height and the patient's weight ($r = 0.67$, $P < .001$). When only the histologically normal adrenal glands were taken into account, the mean height of the caudal pole of the right adrenal gland was 0.58 ± 0.08 cm, and the mean height of the caudal pole for the left adrenal gland was 0.78 ± 0.16 cm.

Invaginations or extensions from the cortex into the medulla were commonly identified on MRI and were histologically diagnosed as a normal anatomical variant. Those were encountered in 50% (31/62) of adrenal glands and in 71% (22/31) of dogs and were found in both histologically normal and diseased adrenal glands from dogs aged between 7 months and 11 years old. On MRI, those invaginations were always smoothly marginated, isointense to minimally hypointense to the cortex on T1W and T2W, and could be found unilaterally (13/22) or bilaterally (9/22) (Figure 1A). On histology, invaginations were identified as regularly organized cortical layers centered around an external fibrous capsule that folded into the medulla and often surrounded a central vessel (Figure 1B).

On histological examination, 72.6% (45/62) of the adrenal glands showed pathological findings, and 27.4% (17/62) were normal. A total of 66 lesions were identified on histology, with 65.4% (29/45) of adrenals glands having one lesion and 35.5% (16/45) having two or three lesions (for example, necrotizing adrenalitis, thrombosis, and hemorrhage). The most common histological diagnosis was cortical hyperplasia, identified in 51.6% (32/62) of adrenal glands. Cortical hyperplasia was categorized as nodular in 62.5% (20/32) of the adrenals and as diffuse in 37.5% (12/32).

On MRI, 82% (51/62) of the adrenal glands were classified as normal, and 18% (11/62) were classified as abnormal. Of those adrenals considered normal on MRI, 68.6% (35/51) were abnormal on histology. All cases considered normal on histology were normal on MRI. Adrenal

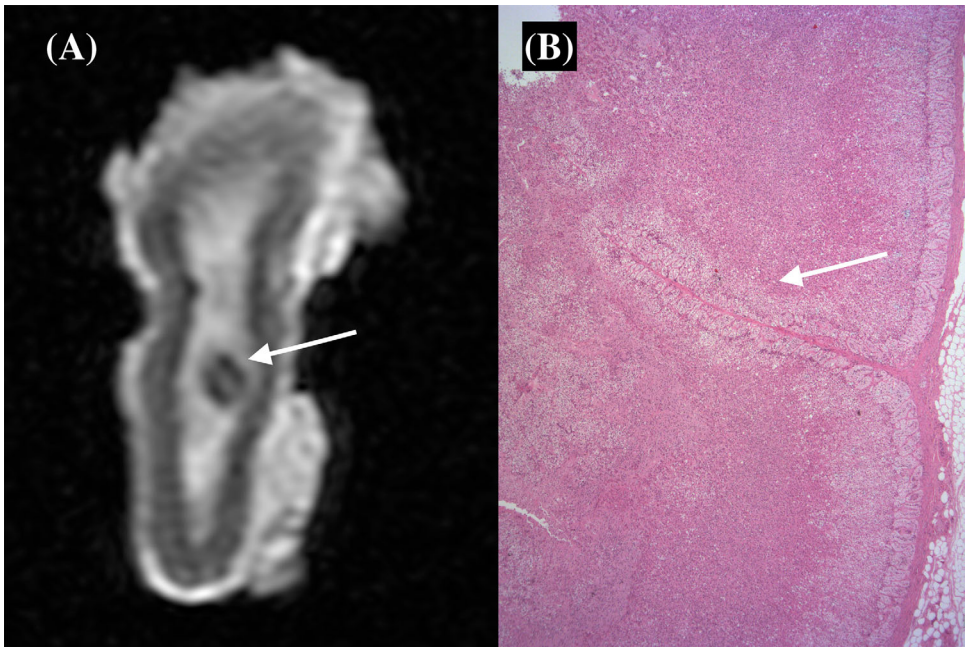

FIGURE 1 A, T2W sequence in the dorsal plane of a normal adrenal gland with a cortical invagination (white arrow). B, Histologic section of the same adrenal gland stained with hematoxylin and eosin shown at 2× magnification. The fibrous capsule folds into the cortex and medulla and is surrounded by the regular organization of cortical layers (white arrow).

lesions were identified on MRI with a sensitivity of 24%, a specificity of 100%, a positive predictive value of 100%, a negative predictive value of 31%, and an accuracy of 45%.

Hyperplasia was identified on MRI in 10 adrenal glands and was most commonly found in older, large-breed dogs. The mean age of those dogs was 8.5 years old (3–12 years old), and the mean body weight was 29.6 kg (13.8–38.5 kg). Among the hyperplastic adrenal glands, the mean height of the caudal pole for the right adrenal gland was 0.76 ± 0.14 cm, and the mean height of the caudal pole for the left adrenal gland was 0.8 ± 0.19 cm. In five of the cases, the hyperplasia was categorized as nodular, and in five cases, as diffuse cortical hyperplasia. On MRI, nodular cortical hyperplasia was identified as small rounded nodular lesions measuring less than 1 cm (0.15–0.9 cm), isointense to the cortex in all sequences, and extending from the cortex toward the medulla. The nodules were better defined as they increased in size and were most commonly multiple. In four out of five cases of nodular cortical hyperplasia, both adrenal glands were affected in the same individual. Diffuse cortical hyperplasia presented in all cases with unilateral involvement and was identified as a focal symmetric or asymmetric thickening of the cortex, with a corresponding narrowed medulla. Diffuse cortical hyperplasia affected the left adrenal gland in three cases and the right adrenal gland in two cases.

The remainder of the lesions identified on MRI included one hemorrhagic nodule, an organized focus of fibrosis, one cortical adenoma, and one hemangiosarcoma. The hemorrhagic nodule (Figure 2A–C) was identified in the cranial pole, affecting both the cortex and medulla and causing mild deformity of the external margin of the cortex. The lesion was ovoidal in shape, measuring 1 cm in maximal dimension. The nodule was heterogeneous, mainly hypointense to the cortex and medulla, and contained multiple foci that were hyperintense in all sequences. The fibrotic nodule was identified as a well-defined, small (0.2 cm in diameter) and rounded lesion, predominantly involving the medulla of the cranial pole, with mild extension to involve the adjacent cortex. The nodule was mildly heterogeneous and strongly hypointense compared with both cortex and medulla in all sequences. The adenoma (Figure 3A, B) was identified as a well-defined ovoid nodule located in the corticomedullary interface of the cranial pole. The nodule measured 0.7 cm in maximal dimension. The nodule was mildly heterogeneous and strongly hypointense compared with both cortex and medulla in all sequences. The hemangiosarcoma was identified as a moderately well-defined small nodule (2.7 mm in diameter) in the lateral cortex of the caudal pole. The nodule was isointense to slightly hyperintense to the cortex and was only visible in the T1W IDEAL sequence (water only) in both the dorsal and transverse planes.

The adrenal signal intensity index was calculated for the hemorrhagic nodule, the fibrotic nodule, and the adenoma, and was between 27.7 and 29.1% in all cases. The signal intensity index of the hemangiosarcoma could not be measured since the nodule could not be identified in the dual-echo sequence.

Five adrenal masses were included from dogs that underwent surgical adrenalectomy. Those masses were diagnosed as one cortical adenoma, one pheochromocytoma, and three adrenocortical carcinomas. The adenoma (Figure 4A–C) was rounded in shape, with an indistinct cortex and medulla, and measured 3.2 cm in length, 2.5 cm in width, and 2.8 cm in height. The mass was mainly T2W and T1W heterogeneously hypointense, with multifocal hyperintense regions that were suppressed in fat saturation sequences.

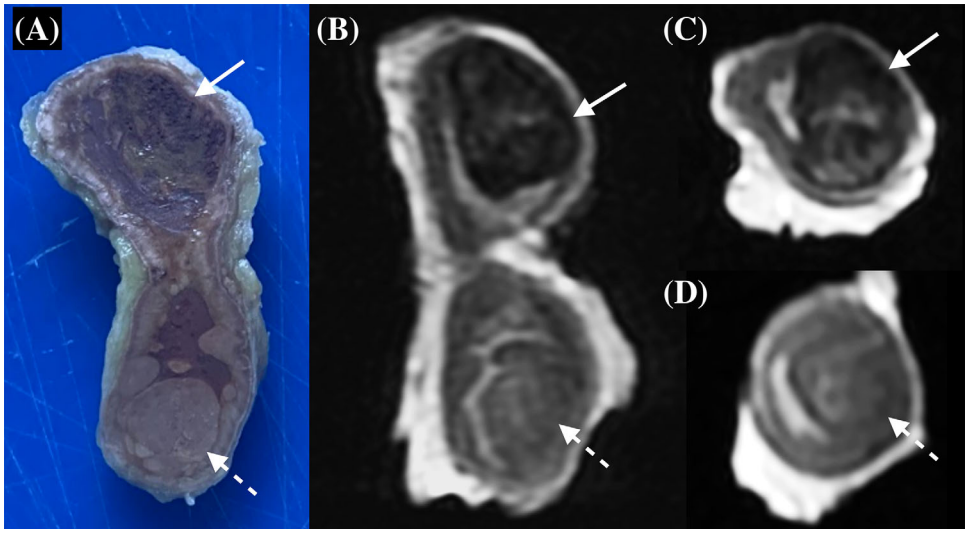

FIGURE 2 A, Gross pathology image of an adrenal gland with a hemorrhagic nodule in the cranial pole (white arrows) and with nodular cortical hyperplasia affecting the caudal pole (dashed arrow). B, T2W sequence in dorsal and (C, D) transverse planes of the same adrenal gland indicating the same hemorrhagic nodule in the cranial pole (white arrows) and the nodular cortical hyperplasia in the caudal pole (dashed arrow).

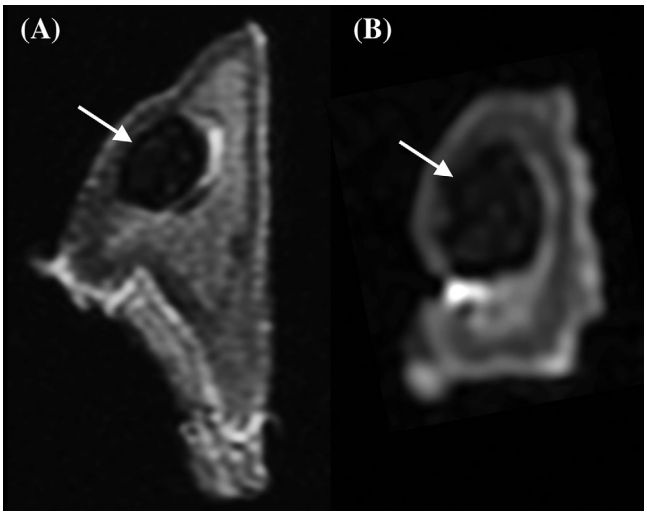

FIGURE 3 A, T2W sequences in dorsal and (B) transverse planes of an adrenal gland with an adenoma on its cranial pole (white arrow).

The pheochromocytoma (Figure 5A, B) was bilobed in shape and measured 6.2 cm in length, 4.7 cm in width, and 3 cm in height. On T2W sequences, the medulla was predominantly hyperintense, and the cortex was hypointense. On T1W sequences, the medulla was mainly hyperintense to the cortex, with only a small, well-defined region that was hypointense. Multiple foci of T2W hypointensity with a signal void on T2*W images were identified within the mass.

The carcinomas (Figure 6A, B) were ovoid ($n = 2$) or bilobed ($n = 1$) in shape. On T2W sequences, all carcinomas had a predominantly heterogeneous and hyperintense medulla and a hypointense cortex. Alternatively, on T1W sequences, the medulla was predominantly hypointense, with a slightly more hyperintense cortex. In all cases, multiple foci of T2W hypointensity were identified, which corresponded to larger areas of signal void in T2*W sequences. In one of the carcinomas, multiple foci of fat intensity were identified within the medulla of the caudal pole, best identified on the T1W IDEAL sequence (fat only). The largest carcinoma measured 9 cm in length, 5.4 cm in width, and 5 cm in height, and the smallest measured 3 cm in length, 1.7 cm in width, and 1.8 cm in height.

The adrenal signal intensity index was calculated for those masses in dual-echo sequences and was between 13% and 21.8% in all cases.

Multiple lesions were not identified on MRI. Those included nodular cortical hyperplasia ($n = 15$), diffuse cortical hyperplasia ($n = 7$), congestion ($n = 7$), hemorrhage ($n = 5$), necrotizing adrenalitis ($n = 5$), thrombi ($n = 3$), amyloidosis ($n = 2$), telangiectasia ($n = 2$), lymphoma ($n = 2$), medullary hyperplasia ($n = 1$), pheochromocytoma ($n = 1$), hemangiosarcoma ($n = 1$), and fibrosis ($n = 1$).

4 | DISCUSSION

Very few studies exist that evaluate canine adrenal glands using MRI. In the present study, the majority of normal adrenal glands presented a hyperintense medulla relative to a hypointense cortex in T2W and T1W. In humans, the abundant vessels and neuroendocrine cells in the medulla are considered to generate the high signal intensity on T2W images, allowing clear delineation of corticomedullary contrast.[18] This may also explain the hyperintensity of the medulla in the present study. Corticomedullary differentiation was possible in all the adrenal glands, best identified on transverse T2W FATSAT, followed by T2W sequence also on the transverse plane. This is in partial agreement with the previous literature. In a previous study in dogs with presumed normal adrenal glands, the cortex and medulla could be differentiated in 51.8% of cases on T2W and T1W sequences, while in 48.2% of the cases, the adrenal glands were homogeneously hypointense.[8] In a more recent study evaluating presumed normal adrenal glands with a 3T MRI unit,[9] the corticomedullary junction was clearly visible on all the 3D

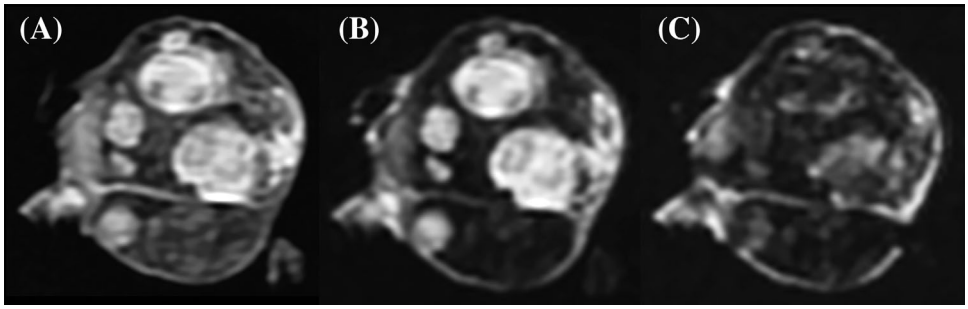

FIGURE 4 A, T1W; B, T2W, and C, T2W fat saturation sequences in dorsal plane of an adrenal adenoma. Note how the hyperintense regions seen on T1W and T2W are suppressed in the fat saturation sequence.

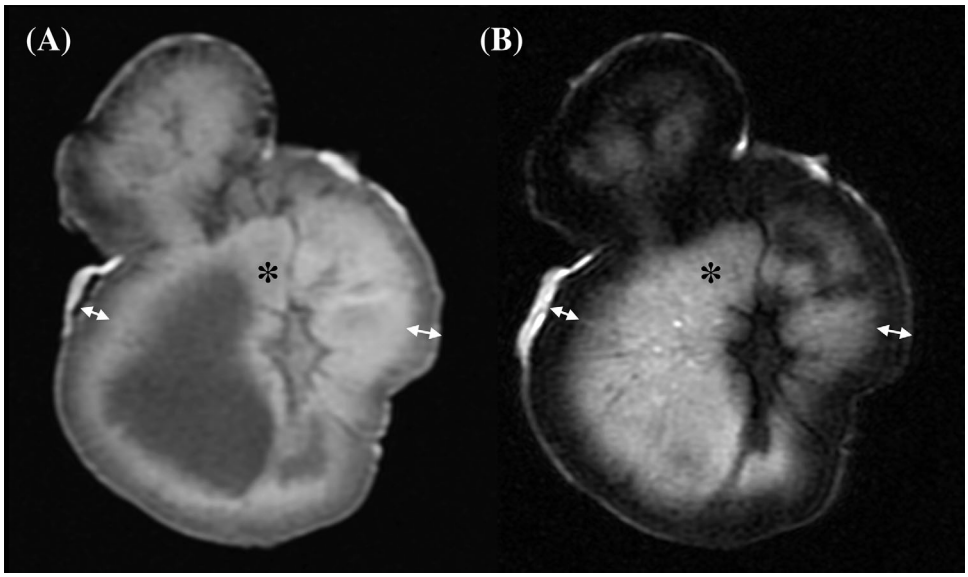

FIGURE 5 A, T1W and B, T2W sequences in dorsal plane of adrenal pheochromocytoma. Note how on both T1W and T2W the medulla (*) is predominantly hyperintense to the adjacent cortex (double arrow).

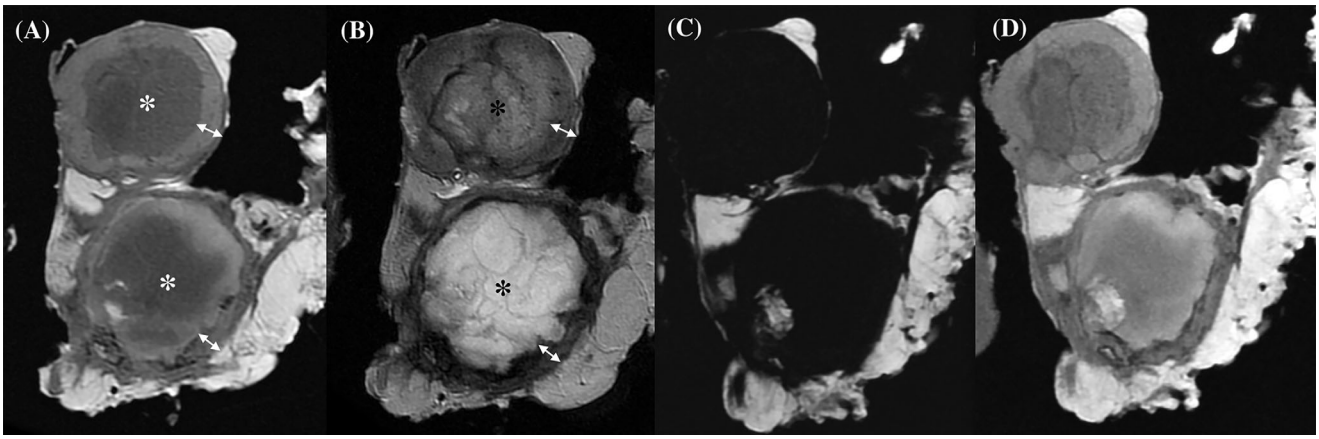

FIGURE 6 A, T1W; B, T2W; C, IDEAL fat only sequence; D, IDEAL fat, and water composition, in the dorsal plane of an adrenal carcinoma. Note how on T1W the medulla (*) is predominantly hypointense to the adjacent cortex (double arrow), while on T2W the medulla (*) is predominantly hyperintense. In IDEAL fat-only sequence the fat is easier to identify with a hyperintense signal, compared with the fat and water composition sequence.

Turbo Spin Echo (TSE) images. Moreover, corticomedullary differentiation was always possible on the 2D TSE sequences in the transverse plane; however, it was not possible in the majority of dogs in the dorsal plane. In the current study, T2W FATSAT and T2W in transverse images were the sequences with a higher repetition time (TR). This could have resulted in a higher signal-to-noise ratio, with a subsequent better corticomedullary differentiation.

The least useful sequence for corticomedullary differentiation was the dual-echo sequence. In human medicine, dual-echo, also known as in-phase and opposed-phase imaging or CSI, is the cornerstone of adrenal MRI. However, in one in vitro study performed in humans evaluating normal adrenal glands, the cortex, and medulla could not be distinguished in any specimen on dual-echo. The authors concluded that CSI does not appear to depict lipids within the cortex of normal adrenal glands as it does with cortical adenomas.[18]

The ability to detect adrenal lesions on MRI in dogs has not been evaluated before. In the current study, MRI showed low sensitivity but high specificity for finding adrenal lesions. Adrenal hyperplasia was the most common radiological finding on MRI. It was also the diagnosis that was most commonly undetected. Of the 32 cases of hyperplasia, only 10 cases were correctly diagnosed on MRI, such that adrenal hyperplasia was undetected in 69% of cases. Despite the small number of cases identified on MRI with nodular cortical hyperplasia, the findings were consistent. The lesions were ovoid in shape, isointense to the cortex, most commonly affecting the adrenal glands bilaterally, and frequently found in older large breed dogs. The mean caudal pole height of the hyperplastic adrenal glands was slightly above the range presented here for histologically normal adrenal glands. Yet, there was an overlap between the measurements, and dogs with hyperplastic adrenals presented greater mean body weight. In cases of unilateral hyperplasia, the caudal pole height of the contralateral adrenal gland was measured and was always within the range of histologically normal adrenal glands reported here. Histological processing methods using formaldehyde and paraffin are known to have mild shrinkage.[19,20] As such, some mild underestimation of adrenal gland size may be present in these processed adrenal glands. Furthermore, in human studies, the use of formaldehyde decreased the MRI relaxation time on T1 and T2 in tissues like the brain or the heart.[21,22] Although these changes have not been studied in fixated adrenal glands, minor alterations in the signal intensity might occur.

In human medicine, adrenal cortical hyperplasia is most often characterized by smooth, diffuse enlargement of the adrenal glands, preservation of normal adrenal shape and signal intensity, and possible presence of various macro- or micronodularity.[23] The most important guide in differential diagnosis, however, is an in-depth clinical evaluation.[23] In the current study, in the absence of historical clinical information, it is uncertain if the lesions identified were of clinical significance.

Interestingly, the two cortical adenomas were hypointense in all the sequences. In human medicine, adenomas have been described as isointense or hypointense to the renal cortex on T2W.[24] Moreover, multiple studies have shown that adenomas have lower T2W signal intensity compared with pheochromocytoma, adrenocortical carcinoma, and metastases.[24] In humans, 70% of adenomas are known to be lipid-rich.[5] Using CSI sequences, qualitative and quantitative assessments of suspected adrenal adenomas are performed. Opposed-phase images are compared with in-phase images to evaluate the signal drop of fat and to calculate a signal intensity index. A signal intensity index higher than 16.5% was postulated to have 100% accuracy in diagnosing lipid-rich adenomas. In contrast, all metastatic tumors had signal intensity indexes of 11.2% or lower.[14] Compared with humans, canine adenomas are suspected to be mostly lipid-poor, which could make the diagnosis difficult.[25] In the present study, the adrenal signal intensity index was calculated for the various nodules and masses. Although the two adenomas had a value over 11.2%, the results were very similar between all lesions, precluding distinction between them.

A small nodular lesion, representing metastasis from splenic hemangiosarcoma, was identified in one adrenal gland. The contralateral adrenal gland had a similar nodule on histology; however, this was not visible on MRI. The cause of this discrepancy is uncertain. A recent study evaluated the veterinary radiologic error rate as determined by necropsy.[26] In that study, the authors classify discrepancies due to sensitivity limitations as those lesions that are too small to be detected by imaging and can only be detected microscopically, regardless of the imaging modality chosen. In the present study, since several lesions could not be visualized retrospectively with the histological comparison alongside, the radiologic-pathologic discrepancies were thought to be due to sensitivity limitations.

The three carcinomas had similar characteristics in signal intensity, being heterogeneous and predominantly hyperintense on T2W and predominantly hypointense on T1W. The MRI features of adrenal carcinomas in dogs have not been previously reported, and the current findings concur with features reported in human medicine. In humans, although the findings are nonspecific, adrenal carcinomas are usually large and heterogeneous, hyperintense on T2W and hypointense on T1W, and may be partially necrotic, hemorrhagic, or calcified.[5,6] The presence of multiple foci of signal void on T2*W sequences, corresponding with T2W hypointense areas in the carcinomas of the present study, were thought to be mineralized foci or regions of chronic hemorrhage. One of the carcinomas had multiple foci of intratumoral fat. In humans, it has been reported that adrenocortical carcinomas and pheochromocytomas can infrequently exhibit focal intratumoral fatty degeneration, mimicking findings of atypical adrenal adenomas or myelolipomas.[5] The authors recommend adding the T1W IDEAL sequence in addition to the conventional T2W and T1W sequences if adrenal masses are encountered for a better evaluation of intratumoral fat infiltration (Figure 6C, D).

The imaging features of pheochromocytomas in humans are also nonspecific.[5,14,27] While 10% of them might have a typical highly hyperintense "lightbulb" appearance on T2W, they can also present necrosis, fibrosis, cystic and fatty degeneration, and calcification, making the diagnosis complex.[5] On T1W, pheochromocytomas are typically isointense to muscle and hypointense to the liver. However, the appearance on T1W is also quite variable if necrosis or hemorrhage is present.[14,27] The pheochromocytoma included in the present study was mainly hyperintense on T2W, with large areas remaining

hyperintense on T1W, which were thought to be due to intratumoral hemorrhage.

The present study has several limitations. The main limitation of the study is the translation of the information obtained from ex vivo adrenal glands to a regular clinical setting. The MR images evaluated in the study were obtained under optimal conditions, with isolated adrenal glands to obtain high-resolution images. In living dogs, high-resolution images may be more time consuming to obtain in clinical scenarios. For example, the effects of patient motion on image quality were not assessed; therefore, this must be considered a preliminary study. Moreover, the ex vivo study design precluded the possibility of contrast media administration, which may affect the sensitivity, specificity, and accuracy of MRI for finding adrenal lesions. The clinical information of the enrolled dogs was limited, and it is unclear if any of the lesions identified were of clinical significance. However, this was outside the scope of the investigation and does not affect the aims of the study. The correlation between the grades provided for corticomedullary differentiation on MRI and the corresponding histology was not assessed. Thus, caution must be taken before arbitrarily using those grades until clinical information can be ascertained. Furthermore, due to the small sample size, multiple histologic diagnoses were presented in only a small number of cases. As a result, a thorough description or possible differentiating traits between diseases was not possible. Another limitation may be that the observer was not blinded when reviewing the MRI studies, and so the sensitivity and accuracy for finding adrenal lesions on MRI may be lower when assessed by blinded observers.

In conclusion, the present manuscript provides information on the MRI appearance of normal and abnormal *ex vivo* adrenal glands of dogs with their corresponding histological comparison. Most adrenal lesions, albeit limited in number, had never been reported in the veterinary literature. While MRI identified numerous adrenal gland lesions, a significant portion of those went undetected. Therefore, the absence of adrenal gland lesions on MRI does not exclude the possibility of histological lesions being present.

ACKNOWLEDGEMENTS

The authors gratefully acknowledge Sean Lacey for his help and expertise in statistical analysis.

LIST OF AUTHOR CONTRIBUTIONS

Category 1

a. Conception and design: Amorós, Hoey
b. Acquisition of data: Amorós, Imlau, Cloack
c. Analysis and interpretation of data: Amorós, Hoey, Imlau, Puggioni, Dalla Serra, Shorten

Category 2

a. Drafting the article: Amorós, Hoey
b. Reviewing article for intellectual content: Amorós, Hoey, Imlau, Puggioni, Dalla Serra, Shorten

Category 3

a. Final approval of the completed article: Amorós, Hoey, Imlau, Puggioni, Dalla Serra, Shorten, Cloack

Category 4

a. Agreement to be accountable for all aspects of the work in ensuring that questions related to the accuracy or integrity of any part of the work are appropriately investigated and resolved: Amorós, Hoey, Imlau, Puggioni, Dalla Serra, Shorten, Cloack

CONFLICT OF INTEREST STATEMENT

The authors declare no conflict of interest.

DATA AVAILABILITY STATEMENT

The data supporting the results of this paper are available from the corresponding author upon reasonable request.

PREVIOUS PRESENTATION OR PUBLICATION DISCLOSURE

Part of the material from this manuscript was presented at the IVRA/EVDI Congress in Dublin, 2023.

EQUATOR NETWORK DISCLOSURE

An EQUATOR network checklist was not used.

ORCID

Olga Amorós Carafí https://orcid.org/0000-0001-5720-9727
Eimear Shorten https://orcid.org/0000-0002-8295-008X
Seamus Hoey https://orcid.org/0000-0003-1049-7658

REFERENCES

1. Gregori T, Mantis P, Benigni L, Priestnall SL, Lamb CR. Comparison of computed tomographic and pathologic findings in 17 dogs with primary adrenal neoplasia. *Vet Radiol Ultrasound*. 2015;56(2):153-159.
2. Caoili EM, Korobkin M, Francis IR, et al. Adrenal masses: characterization with combined unenhanced and delayed enhanced CT. *Radiology*. 2002;222(3):629-633.
3. Foti G, Faccioli N, Mantovani W, Malleo G, Manfredi R, Mucelli RP. Incidental adrenal lesions: accuracy of quadriphasic contrast enhanced computed tomography in distinguishing adenomas from nonadenomas. *Eur J Radiol*. 2012;81(8):1742-1750.
4. Blake MA, Kalra MK, Sweeney AT, et al. Distinguishing benign from malignant adrenal masses: multi-detector row CT protocol with 10-minute delay. *Radiology*. 2006;238(2):578-585.
5. Adam SZ, Nikolaidis P, Horowitz JM, et al. Chemical shift MR imaging of the adrenal gland: principles, pitfalls, and applications. *Radiographics*. 2016;36(2):414-432.
6. D'amuri FV, Maestroni U, Pagnini F, et al. Magnetic resonance imaging of adrenal gland: state of the art. *Gland Surg*. 2019;8(3):S223. Suppl.
7. Yoshida O, Kutara K, Seki M, Ishigaki K, et al. Preoperative differential diagnosis of canine adrenal tumors using triple-phase helical computed tomography. *Vet Surg*. 2016;45(4):427-435.
8. Llabres-Diaz FJ, Dennis R. Magnetic resonance imaging of the presumed normal canine adrenal glands. *Vet Radiol Ultrasound*. 2003;44(1):5-19.

9. Lee E, Choi BK, Lee SK, Choi J. 3.0-Tesla MRI of normal canine adrenal glands. *Vet Radiol Ultrasound*. 2022;63(2):206-215.
10. Spall B, Chen AV, Tucker RL, Lahmers KK, Righter DJ, Hayles J. Imaging diagnosis—metastatic adrenal pheochromocytoma in a dog. *Vet Radiol Ultrasound*. 2011;52(5):534-537.
11. Manley R, Matthews AR, Morandi F. Magnetic resonance imaging of the canine abdomen: effect of pulse sequence on diagnostic quality. *Vet Radiol Ultrasound*. 2013;54(3):253-262.
12. Maxie G. *Jubb, Kennedy & Palmer's pathology of domestic animals*. Elsevier Health Sciences; 2015; volume.
13. Zachary James F. *Pathologic basis of veterinary disease/James F. Zachary, M. Donald McGavin. St. Louis*. Elsevier; 2012;951-952.
14. Fujiyoshi F, Nakajo M, Fukukura Y, Tsuchimochi S. Characterization of adrenal tumors by chemical shift fast low-angle shot MR imaging: comparison of four methods of quantitative evaluation. *Am J Roentgenol*. 2003;180(6):1649-1657.
15. Agut A, Martinez M, Anson A, Soler M. Ultrasonographic measurement of adrenal gland-to-aorta ratio as a method of estimating adrenal size in dogs. *Vet Rec*. 2020;186(19):e27.
16. Pagani E, Tursi M, Lorenzi C, Tarducci A, et al. Ultrasonographic features of adrenal gland lesions in dogs can aid in diagnosis. *BMC Vet Res*. 2016;12:1-9.
17. Perfetti S, Diana A, Baron Toaldo M, Cipone M, Quinci M, Pey P. CT measures of adrenal gland length and caudal pole diameter are reproducible in large breed dogs: a pilot study. *Vet Radiol Ultrasound*. 2021;62(4):402-412.
18. Mitchell DG, Nascimento AB, Alam F, Grasel RP, Holland G, O'hara BJ, Normal adrenal gland: in vivo observations, and high-resolution in vitro chemical shift MR imaging–histologic correlation. *Acad Radiol*. 2002;9(4):430-436.
19. Bahr GF, Bloom G, Friberg U. Volume changes of tissues in physiological fluids during fixation in osmium tetroxide or formaldehyde and during subsequent treatment. *Exp Cell Res*. 1957;12(2):342-355.
20. Penttila A, McDowell EM, Trump BF. Effects of fixation and postfixation treatments on volume of injured cell. *J Histochem Cytochem*. 1975;23(4):251-270.
21. Dawe RJ, Bennett DA, Schneider JA, Vasireddi SK, Arfanakis Konstantinos. Postmortem MRI of human brain hemispheres: t2 relaxation times during formaldehyde fixation. *Magnetic Resonance Med*. 2009;61(4):810-818.
22. Ebata K, Noriki S, Inai K, Kimura H. Changes in magnetic resonance imaging relaxation time on postmortem magnetic resonance imaging of formalin-fixed human normal heart tissue. *BMC Med Imaging*. 2021;21:1-2.
23. Michelle AM, Jensen CT, Habra MA, et al. Adrenal cortical hyperplasia: diagnostic workup, subtypes, imaging features and mimics. *Br J Radiol*. 1079;90:20170330.
24. Tu W, Gerson R, Abreu-Gomez J, Udare A, Mcphedran R, Schieda N. Comparison of MRI features in lipid-rich and lipid-poor adrenal adenomas using subjective and quantitative analysis. *Abdominal Radiol*. 2021;46(10):4864-4872.
25. Morandi F, Mays JL, Newman SJ, Adams WH. Imaging diagnosis—bilateral adrenal adenomas and myelolipomas in a dog. *Vet Radiol Ultrasound*. 2007;48(3):246-249.
26. Cohen J, Fischetti AJ, Daverio H. Veterinary radiologic error rate as determined by necropsy. *Vet Radiol Ultrasound*. 2023;64(4):573-584.
27. Leung K, Stamm M, Raja A, Low G. Pheochromocytoma: the range of appearances on ultrasound, CT, MRI, and functional imaging. *Am J Roentgenol*. 2013;200(2):370-378.

SUPPORTING INFORMATION

Additional supporting information can be found online in the Supporting Information section at the end of this article.

How to cite this article: Carafí OA, Imlau M, Dalla Serra G, et al. Ex vivo MRI and histological comparison of the canine adrenal glands. *Vet Radiol Ultrasound*. 2024;1-10. https://doi.org/10.1111/vru.13425